SUPPORTING INFORMATION

I. Simulation of bi-layer capacitors from Landau Theory

Landau theory[1], and its subsequent application to ferroelectric material[2], describes the energy density in a non-linear insulator. The energy function is expressed as an even series expansion of the order parameter polarization (P), coupled with material coefficients as

$$U = t_1(\alpha_1 P^2 + \beta_1 P^4 + \gamma_1 P^6) \qquad (S1)$$

where t_1 is the thickness of capacitor C_1, and α_1, β_1, γ_1, are the material coefficients that describe the properties of C_1. We obtain U as a surface energy density with the thickness of the capacitor multiplied across. For a bi-layer structure consisting of two separate material, two thicknesses contribute to the insulating layer of the MIM capacitor. Equation S1 can be modified in order to attribute both energy density functions from C_1 and C_2 in the bilayer

$$U_T = t_1(\alpha_1 P^2 + \beta_1 P^4 + \gamma_1 P^6) + t_2(\alpha_2 P^2 + \beta_2 P^4 + \gamma_2 P^6) \qquad (S2)$$

where a second capacitance C_2 has been summed to the original energy function creating a total energy density U_T. Equation S2 is now a combination of a $SrTiO_3$ layer as capacitor C_1, and a $BaTiO_3$ layer constituting C_2, creating the overall insulating thickness in the MIM stack.

Minimizing equation S2 to find the stable operating points at the minima of energy we find

$$\delta U_T / \delta P = E = 0 = t_1(2\alpha_1 P + 4\beta_1 P^3 + 6\gamma_1 P^5) + t_2(2\alpha_2 P + 4\beta_2 P^3 + 6\gamma_2 P^5) \qquad (S3)$$

which can be simulated to acquire polarization - electric field bias (E) loops in the bi-layer structure. Differentiating equation S3 allows the expected capacitance to be derived, which is fully consistent with a scaled version of capacitance, C = dq/dV, where q is charge, V is voltage.

Simulations based upon energy density functions in equation S1, S2, and polarization - electric field relationships from equation S3, are given in Figure S1. Values for material coefficients are given in ref. 1, including Curie temperature for $BaTiO_3$ and $SrTiO_3$ of 388 K and 35.5 K, respectively. The figure presents a simulation for both a single $SrTiO_3$ (C_1) and $BaTiO_3$ (C_2) layer, in addition to a bi-layer (C_T) comprising the summation of the contributing energy two functions. Capacitance relationships are derived from the polarization loops. At a temperature of 100 K, Figure S1(a) shows C_2 with deep energy minima. The resulting summation with the energy function in C_1 produces a bi layer function with remaining negative energy. The consequence of this on the polarization response is hysteresis, and the negative slope around zero bias is unstable. Hysteretic jumps in polarization will ensue in a bi-layer at this temperature; hence negative capacitance remains unstable.

For a temperature of 300 K, the resulting summation of energy from C_1 and C_2 produce an overall single minimum positive energy function for C_T (Figure S1(b)). Further to this, the total energy function is shallower than C_1. The implications on capacitance show that C_T is measured greater than C_1 due to the contributing negative capacitance in C_2. This will only be measured in a system comprising a positive capacitor in series with a negative one.

Raising the temperature to 500 K, both contributing capacitors C_1 and C_2 are paraelectric, and hence any negative capacitance property is lost in the ferroelectric layer (Figure S1(c)). The total capacitance is now lower that the smallest of the two layers, $C_T < C_1, C_2$. This results from standard analysis of two positive series capacitors.

The above discussion places temperature as an important parameter. It is well known that ferroelectric material are responsive to temperature, and change in phase at a given critical point, T_c. Moving towards T_c, the double well energy minima decrease and transition

toward a single minimum at zero P. In turn, this reduces the window of negative capacitance (Figure S1(a)), and summation of a positive energy function must be balanced correctly if a total energy function is to be stabilised to produce $C_T > C1$. As equation S3 shows, the thickness of the constituent capacitors C_1 and C_2 can be selected in order to stabilise the system at a given temperature. Designing the thickness of the bi-layer, and taking into account the parameter T_c of the ferroelectric material allows stabilisation of negative capacitance at room temperature in $BaTiO_3$. Further influences from straining in epitaxial films that are clamped to a substrate may impact the energy density in equation S3. The misfit strain imposed on the grown films can lead to a critical temperature that shifts under the influence of the strain. For the case of $BaTiO_3$ grown on $SrTiO_3$ under investigation here, a negative value of misfit strain will act to favour the c-phase[3]. This phase shows out-of-plane polarization $P_3 \neq 0$, and in-plane contributions $P_1 = P_2 = 0$, and is most desirable for the negative capacitance stabilisation in the bi-layer.

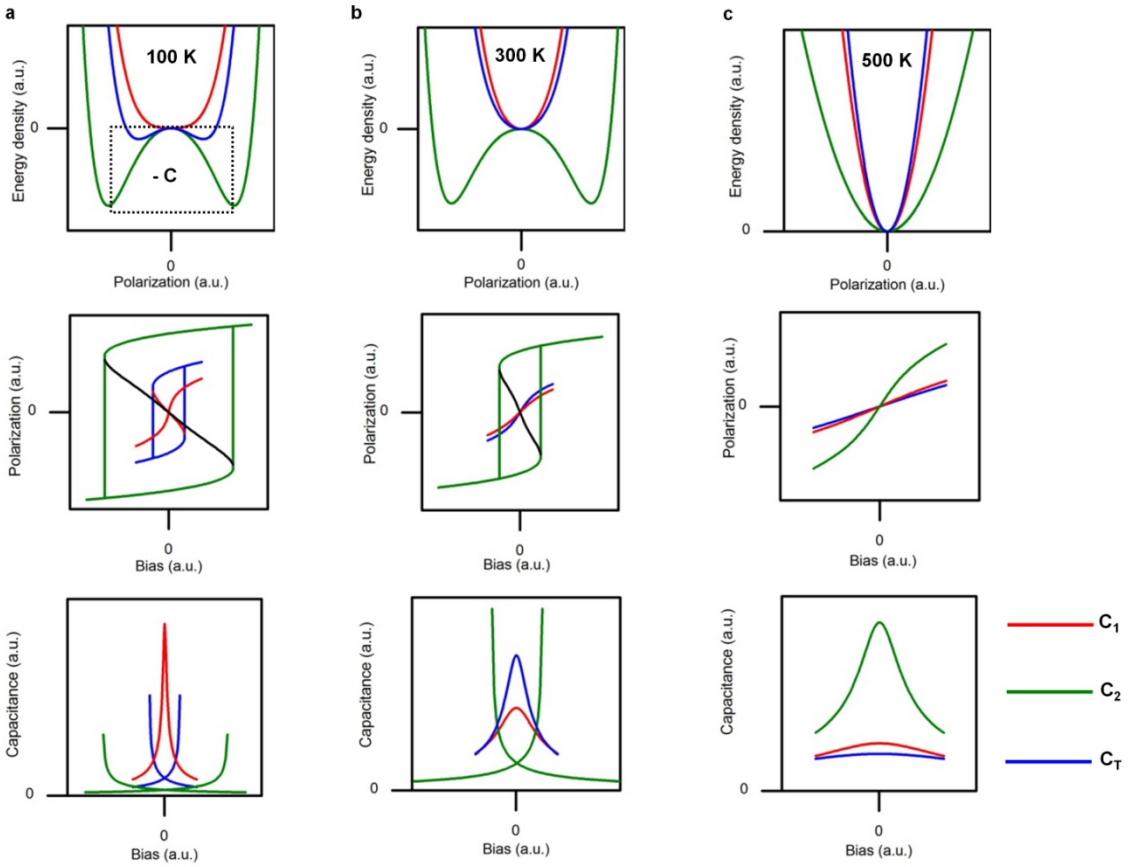

Figure S1. Energy density functions, polarization - bias, and capacitance - bias simulations of $SrTiO_3$ (C_1), $BaTiO_3$ (C_2), and bi-layer (C_T). **a,** simulation at 100 K. C_T remains unstable with hysteretic polarization. **b,** simulation at 300 K. Stabilisation in C_T is apparent and the overall capacitance is measured greater than the constituent C_1 capacitance. **c**, simulation at 500 K. The system is a contribution of two paraelectric material and negative capacitance is lost. C_T is measured smaller than both constituent capacitances.

II. X-Ray Diffraction and Atomic Force Microscopy

X-Ray diffraction data for both the $SrTiO_3$ 25 nm capacitor C_1, and bilayer C_T of 25 nm $SrTiO_3$ / 50 nm $BaTiO_3$ are shown in Figure S2. It is observed that the structures are epitaxially grown in (100) orientation, as set by the single crystal $SrTiO_3$ (100) substrate, with peak positions indicating the perovskite phase. The spectra of the remaining structures are shown in Figure S3. The well matched lattice constants allows coherent growth of a full perovskite structure with atomically smooth interfaces. The surface roughness is measured using atomic force microscopy in Figure S4. The results consist of (10 x 10) μm surface topography scans of C_1 25 nm $SrTiO_3$, and C_T 25 nm / 50 nm $SrTiO_3$ / $BaTiO_3$ bi-layer. In Figure S4(a) for C_1, the surface shows to be smooth and uniform, lacking any indication of grain structure and resulting grain boundaries. Calculated root mean square surface roughness was 0.5 nm. Figure S4(b) shows the matching surface scan for C_T, $SrTiO_3$ / $BaTiO_3$. The results are directly comparable to that in the $SrTiO_3$ image shown in Figure S4(a) in that the surface is smooth and uniform, with no apparent grain structure. Calculated surface roughness for the bilayer was 0.9 nm.

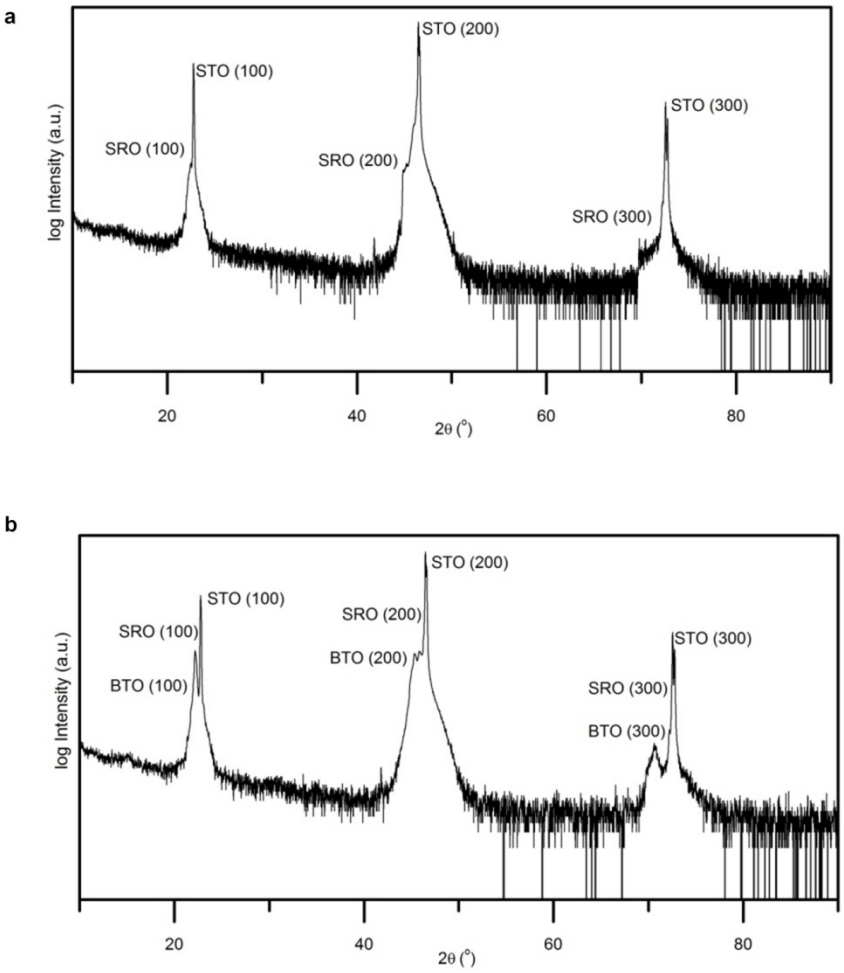

Figure S2. X-Ray diffraction spectra of two of the structures under investigation. **a,** $SrTiO_3$ 25 nm capacitor C_1. **b,** bi-layer C_T of 25 nm $SrTiO_3$ / 50 nm $BaTiO_3$. Each spectra shows the single crystal perovskite phase of the material under investigation.

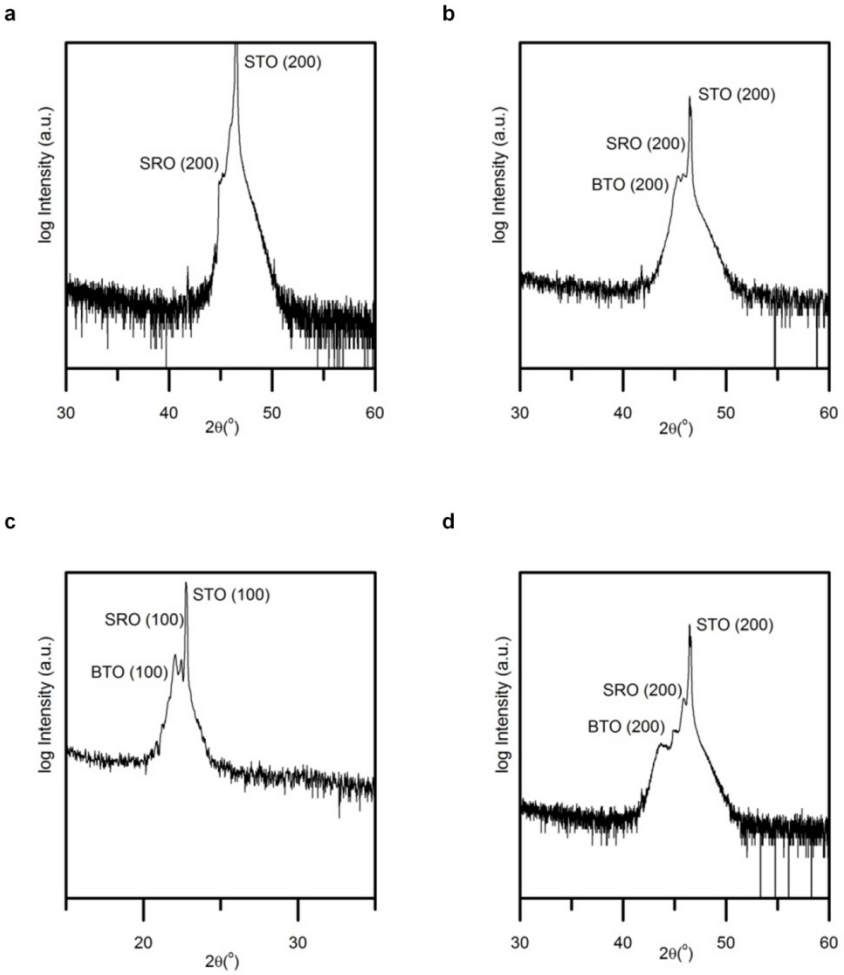

Figure S3. X-Ray diffraction spectra of the structures under investigation. **a,** $SrTiO_3$ 25 nm capacitor C_1. **b,** bi-layer C_T of 25 nm $SrTiO_3$ / 50 nm $BaTiO_3$. **c,** bi-layer C_T of 25 nm $SrTiO_3$ / 30 nm $BaTiO_3$. **d,** bi-layer C_T of 25 nm $SrTiO_3$ / 20 nm $BaTiO_3$.

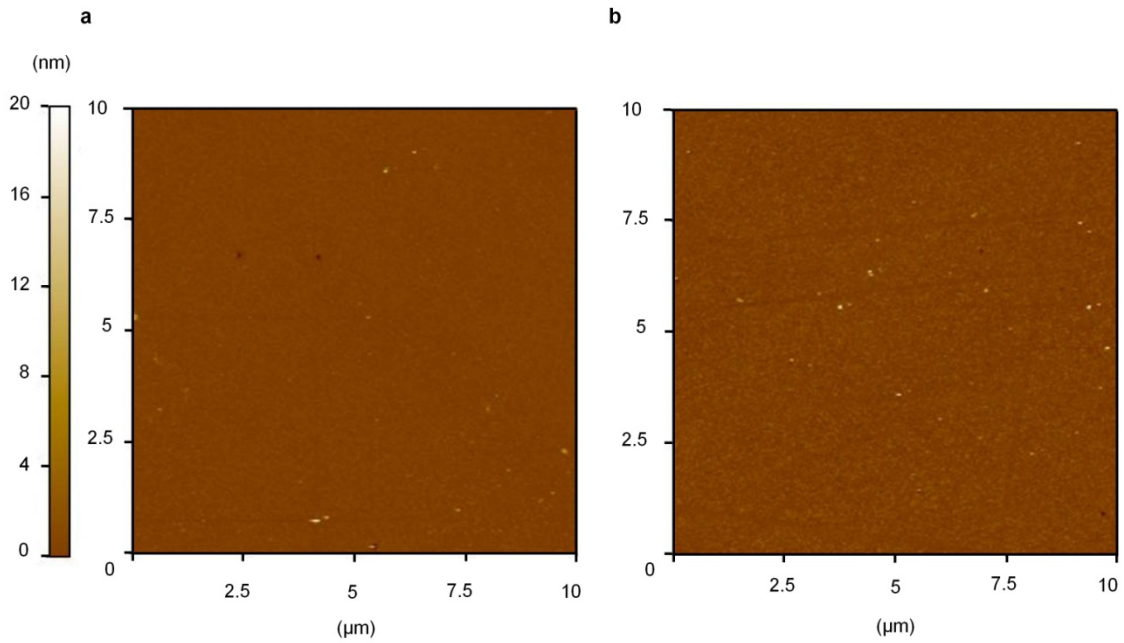

Figure S4. Atomic force microscopy topography scans of two of the structures under investigation. **a,** $SrTiO_3$ 25 nm capacitor C_1. **b,** bi-layer C_T of 25 nm $SrTiO_3$ / 50 nm $BaTiO_3$.

III. Frequency response

Capacitance measured as a function of frequency in C_T and C_1 is shown in Figure S5. In order to discount Maxwell-Wagner (MW) effects, and any defect influences, the frequency is swept from 1 kHz up to 1 MHz. The bi-layer capacitance is seen to be greater than C_1 over the full range of measured frequency. This leads to the conclusion that the capacitance enhancement is originating from a stabilised negative capacitance in C_2.

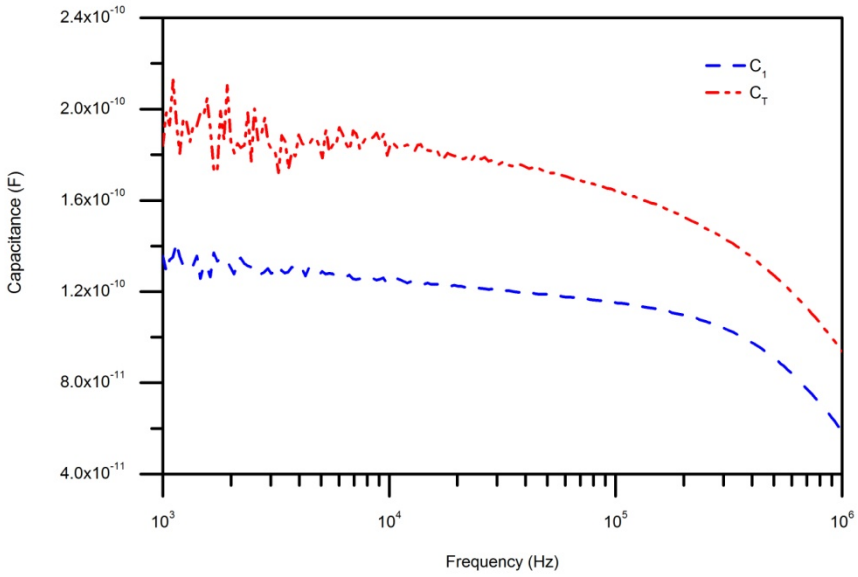

Figure S5. Capacitance as a function of frequency in $SrTiO_3$ 25 nm capacitor C_1 and bi-layer C_T of 25 nm $SrTiO_3$ / 30 nm $BaTiO_3$.

IV. Piezoforce Microscopy

A single layer of $BaTiO_3$ of thickness 30 nm was grown epitaxially on $SrRuO_3$. It was characterized using piezoforce microscopy in order to confirm the ferroelectric behaviour of the pulsed laser deposited grown thin film. The amplitude of the piezoresponse was measured using piezoforce microscopy and is shown in Figure S6. Piezoforce spectra were acquired using a Park Systems XE 150 AFM and the cantilever used was NSC 36 Ti/Pt b. The electric field was swept from −700 kV/cm to +700 kV/cm and vice versa. The alternating voltage applied to the tip had an amplitude of 0.8 V, and a frequency of 20 kHz. The amplitude of the cantilever oscillation was read using a Stanford Research Systems DSP lock-in amplifier, model SR830. The piezoforce spectrum demonstrates the ferroelectric characteristic of the $BaTiO_3$ film with symmetrical coercive fields of ±350 kV/cm. An increase in the piezoresponse after the coercive field for forward and reverse sweeps (indicated by arrows) shows the ferroelectric domain reversal[4].

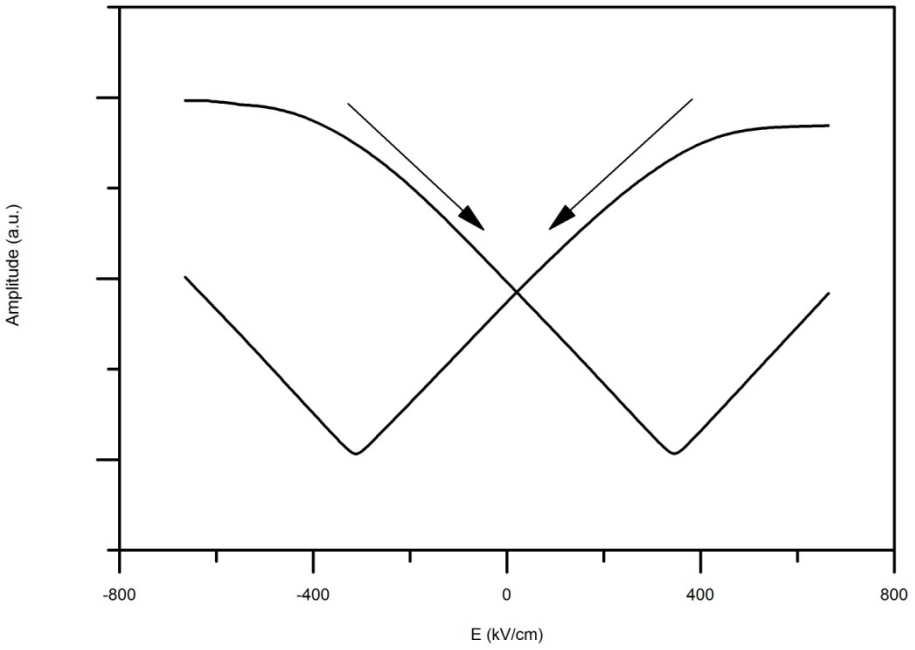

Figure S6. Piezoforce microscopy measurement in 30 nm C_2 capacitor as a function of applied electric field. Arrows indicate the direction of the applied electric field.

References

1. Rabe, K. Ahn, C. H. & Triscone, J.-M. Physics of Ferroelectrics: A Modern Perspective. *Topics Appl. Physics,* **2007,** 105.
2. Devonshire, A. F. Theory of barium titanate. *Philos. Mag*. **1949,** 40, 1040-1063.
3. Pertsev, N. A., Zembilgotov, A. G. & Tagantsev, A. K. Effect of Mechanical Boundary Conditions on Phase Diagrams of Epitaxial Ferroelectric Thin Films. *Phys. Rev. Lett.* **1998,** 80.
4. Kalinin, S. V., Morozovska, A. N., Chen, L. Q. & Rodriguez, B. J. Local polarization dynamics in ferroelectric materials. *Reports Prog. Phys.* **2010**, 73, 056502.